Structural effects on the magnetic and transport properties of perovskite $A_{1-x}A'_xMnO_3$ ($x=0.25$, 0.30)

P. G. Radaelli and G. Iannone
Institut Max Von Laue-Paul Langevin, Boîte Postale 156, 38042 Grenoble Cedex 09, France

M. Marezio
MASPEC-CNR, via Chiavari 18A, 43100 Parma, Italy

H. Y. Hwang and S-W. Cheong
Bell Laboratories, Lucent Technologies, Murray Hill, New Jersey 07974

J. D. Jorgensen and D. N. Argyriou*
Materials Science Division, Argonne National Laboratory, Argonne, Illinois 60439
(Received 22 April 1997)

The evolution of the structural properties of $A_{1-x}A'_xMnO_3$ was determined as a function of temperature, average A-site radius $\langle r_A\rangle$, and applied pressure for the ''optimal'' doping range $x=0.25$, 0.30, by using high-resolution neutron powder diffraction. The metal-insulator transition, which can be induced both as a function of temperature and of $\langle r_A\rangle$, was found to be accompanied by significant structural changes. Both the paramagnetic charge-localized phase, which exists at high temperatures for all values of $\langle r_A\rangle$, and the spin-canted ferromagnetic charge-ordered phase, which is found at low temperatures for low values of $\langle r_A\rangle$, are characterized by large metric distortions of the MnO_6 octahedra. These structural distortions are mainly incoherent with respect to the space-group symmetry, with a significant coherent component only at low $\langle r_A\rangle$. These distortions decrease abruptly at the transition into the ferromagnetic metal phase. These observations are consistent with the hypothesis that, in the insulating phases, lattice distortions of the Jahn-Teller type, in addition to spin scattering, provide a charge-localization mechanism. The evolution of the average structural parameters indicates that the variation of the electronic bandwidth is the driving force for the evolution of the insulator-to-metal transition at T_C as a function of ''chemical'' and applied pressure. [S0163-1829(97)02737-9]

I. INTRODUCTION

An intense research effort has recently been devoted to studying the interplay between structure, magnetism, and transport in manganese perovskites $A_{1-x}A'_xMnO_3$ (A=La, rare earth, A'=Ca,Sr,Ba).[1–9] As a function of temperature, applied magnetic field, doping, applied pressure, A-site ionic radius $\langle r_A\rangle$, and A-site size disorder, this system displays a rich phase diagram for both magnetotransport and structural properties. In the absence of charge carriers ($x=0$), this compound is an antiferromagnetic insulator,[10,11] although its magnetic structure (known as an A-type structure), being made of ferromagnetic MnO_2 planes coupled antiferromagnetically along the b axis,[12] implies the existence of both ferromagnetic and antiferromagnetic interactions between Mn spins. Upon substitution of a divalent alkaline-earth metal (Ca,Sr,Ba) for a trivalent rare earth or lanthanum on the perovskite A site, a certain percentage of Mn^{3+} is formally replaced with Mn^{4+} (electronic doping), providing potential charge carriers for electrical conductivity. For certain values of the electronic doping and of the A-site ionic radius, these compounds are metallic and ferromagnetic at low temperatures, while their conductivity displays semiconducting behavior at high temperatures. The metal-insulator transition between these two states is strongly coupled with the magnetic ordering transition. The metal-insulator transition temperature $T_{M\text{-}I}$ coincides with the Curie temperature T_C. Therefore, for temperatures in the vicinity of T_C, a strong variation of the electrical resistivity, up to several orders of magnitude, occurs upon application of a magnetic field of a few tesla, a phenomenon that has become known as colossal magnetoresistance. The nature of the low-temperature ferromagnetic metal phase, and the coupling between T_C and $T_{M\text{-}I}$ were discussed in 1951 by Zener,[13] who proposed the so-called double-exchange mechanism.[14,15] In Zener's model, ferromagnetic alignment of the Mn magnetic moment is favored by coupling through the conduction electrons. Furthermore, above T_C, charge carriers are localized through scattering by the Mn spins, in the context of strong on-site Hund's rule coupling. Upon the more recent renaissance of manganite research, in spite of the effort to adapt the theoretical description of the double-exchange model to the new experimental data,[16] the validity of this latter assumption has been called into question. In fact, some authors have proposed that double exchange alone is unable to explain either the value of T_C (which should be much higher), or the absolute value and the temperature dependence of the electrical resistivity above T_C.[17–19] For these reasons, the nature of the charge-carrier localization mechanism in the paramagnetic phase is perhaps the most important issue in the physics of these materials.

Among the possible mechanisms for charge localization, lattice distortions due to the different ionic radii of Mn^{3+} and Mn^{4+} and to the tendency of Mn^{3+} to assume a Jahn-Teller-distorted configuration have received a considerable attention.[17–19] In particular, some authors have proposed that, above T_C, charge may be localized in the form of ''JT polarons.'' In this scenario, JT distortion of the $Mn^{3+}O_6$ octahedra should be present in the paramagnetic phase but absent in the low-temperature metallic phase. However, it is clear that, at least in the case of the compositions with the highest T_C, these distortions cannot be coherent with respect to the crystallographic space group symmetry ($R3c$), which imposes on average identical and metrically undistorted MnO_6 octahedra. Strong supporting evidence that partially incoherent structural distortions are involved in the M-I transition has been recently provided by the observation of an abrupt reduction of the oxygen Debye-Waller factors at T_C on cooling,[5,20–22] which is accompanied, in the orthorhombic phase, by a decrease of the (small) coherent component of the JT distortion.[5]

Crystallographic techniques can measure the full extent of these lattice distortions only for phases, like $LaMnO_3$,[10,11] which display *coherent orbital ordering*. Therefore, a key role in the understanding of the relationships between *local* and *average* structure is played by the so-called charge-ordered compounds, like $La_{0.5}Ca_{0.5}MnO_3$ (Refs. 5 and 23) or $Pr_{0.7}Ca_{0.3}MnO_3$.[24–27] In the case of $La_{0.5}Ca_{0.5}MnO_3$, it has been shown[9] that charge and magnetic ordering are associated with orbital ordering, whereby the JT-distorted $Mn^{3+}O_6$ octahedra form a long-range-ordered quasicommensurate superstructure. We will argue in the remainder of this paper that, based on the similarities of the average structure, a similar but *short-range-ordered* arrangement may be present in the paramagnetic phase. This is the first important reason to study the evolution of the *average* structural parameters across the phase diagram in general, and through the M-I and charge-ordering transitions in particular.

A second but no less important reason to analyze systematically the crystal structure of the manganites is understanding the basic mechanism by which the magnetotransport properties can be ''tuned'' at constant doping. It has been shown that T_C is very sensitive to both ''chemical'' pressure (i.e., structural distortions induced by changing $\langle r_A \rangle$),[1,7,8] and applied pressure.[2,28,29] It has been proposed that these effects are related to changes of the charge-carrier bandwidth W, which describes electron hopping from the Mn sites. Preliminary data[1] have evidenced, as a function of $\langle r_A \rangle$, large changes of the Mn-O-Mn angles, which are presumed to affect W. In the present work, a comprehensive study of these effects is presented.

In this paper, we present a systematic neutron powder-diffraction study of the structural and magnetic properties of $A_{1-x}A'_xMnO_3$ (A=Pr, La, A'=Ca, Sr, Ba, x=0.25, 0.30) as a function of temperature, A-site ionic radius $\langle r_A \rangle$, and applied pressure, spanning across the three magnetotransport phases (paramagnetic semiconductor, ferromagnetic metal, and charge-ordered spin-canted insulator), and across the three crystallographic phase regions (*Pnma*, $R3c$, and *Imma*, see Ref. 6), which are found for these doping levels. By correlating ''chemical'' pressure and applied pressure data, we investigate the influence of both Mn-O-Mn angles and Mn-O bond lengths upon the magnetic and transport properties. Furthermore, we show the existence of structural similarities between the spin-canted, charge-ordered insulating phase (which is present at low temperatures for small $\langle r_A \rangle$) and the paramagnetic semiconductor phase (found for larger $\langle r_A \rangle$ above T_C). Both phases are characterized by a coherent JT distortion of the MnO_6 octahedra and by large Debye-Waller factors, which are both abruptly reduced by crossing the phase boundaries into the metallic phase.

II. SYNTHESIS AND NEUTRON POWDER DIFFRACTION

Polycrystalline samples of $A_{1-x}A'_xMnO_3$ (A=La, Pr, A'=Ca, Sr, Ba, x=0.25, 0.3) were synthesized through conventional solid-state reaction in air. The samples of the $A_{0.7}A'_{0.3}MnO_3$ series, with compositions $Pr_{0.7}Ca_{0.3}MnO_3$, $La_{0.525}Pr_{0.175}Ca_{0.3}MnO_3$, $La_{0.7}Ca_{0.17}Sr_{0.13}MnO_3$, $La_{0.7}Ca_{0.13}Sr_{0.17}MnO_3$, $La_{0.7}Sr_{0.3}MnO_3$, $La_{0.7}Sr_{0.12}Ba_{0.18}MnO_3$, and $La_{0.7}Ba_{0.3}MnO_3$ and masses of 1–2 g, are the same used for the work reported in Refs. 1 and 6. For the study of the structural anomalies at T_C, a large $La_{0.75}Ca_{0.25}MnO_3$ sample (20 g) was prepared by the same technique (preliminary data collected from the same sample was reported in Ref. 5). This slightly different doping value was chosen because, at this composition, we have previously observed the presence of lattice constant anomalies at $T_C \approx 240$ K (Ref. 4). Neutron powder-diffraction data were collected on the $A_{0.7}A'_{0.3}MnO_3$ samples at ambient pressure, at 1.6 and 300 K, using the D2B diffractometer of the Institute Laue-Langevin, equipped with a standard ''orange'' cryostat, at a wavelength of 1.594 Å and with no primary beam collimation (the monochromator mosaic spread full width at half maximum being $\sim 15'$ of arc) and $5'$ collimation between sample and detector. High-pressure neutron powder-diffraction data were collected on the same samples at room temperature and at pressures between 0 and 0.6 GPa, using the time-of-flight special environment powder diffractometer at the intense pulsed neutron source of Argonne National Laboratory, equipped with a helium gas cell. Structural parameters were refined by the Rietveld method, using the program GSAS.[30] For each composition, $\langle r_A \rangle$ was calculated using the tabulated values of Ref. 31 for atoms in ninefold coordination (for details, see Sec. IV). Temperature-dependent neutron powder-diffraction data ($20 \leqslant T \leqslant 400$ K) were obtained on the $La_{0.75}Ca_{0.25}MnO_3$ sample using D2B equipped with an ILL cryofurnace. Since for this composition the *metric* distortion from a tetragonal unit cell is very small ($a \approx c$), particular care was taken to optimize the resolution. Therefore, for each temperature, data were obtained at two different wavelengths ($\lambda_1 = 1.594$ Å, $\lambda_2 = 2.400$ Å). The λ_2 wavelength was filtered using a 3 cm thick highly oriented pyrolitic graphite filter in the primary beam ($\lambda/2$ and $\lambda/3$ contamination were lower than 0.1% and 0.2%, respectively). Furthermore, for both wavelengths, the monochromatic beam divergence α_2 was limited to $\sim 0.2°$, by means of a slit system positioned ~ 15 cm after the monochromator (the same configuration as for the other data was used for the primary beam and detector collimation). Data sets at the two wavelengths were simultaneously refined using the program GSAS. As an example, the Rietveld plots for

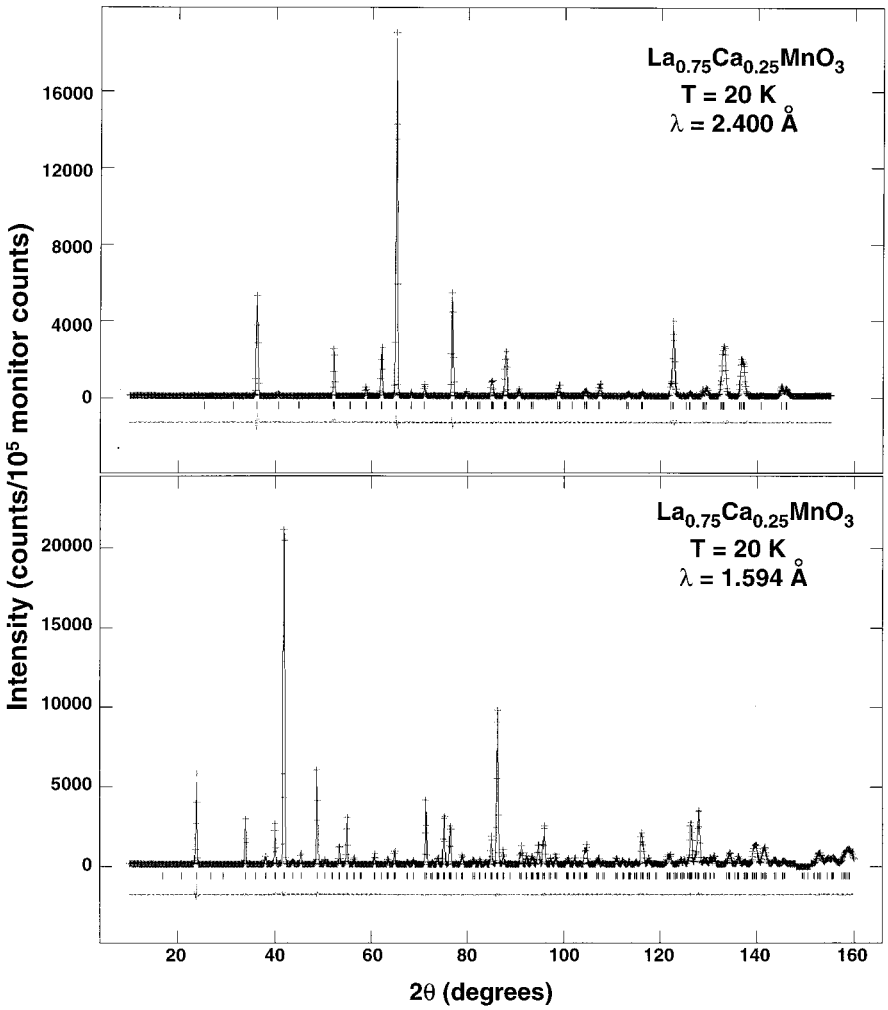

FIG. 1. Rietveld plots of neutron powder-diffraction data at $\lambda_1 = 1.594$ Å (bottom) and $\lambda_2 = 2.400$ Å (top) for $La_{0.75}Ca_{0.25}MnO_3$ at 20 K. The plus (+) signs are raw data (the background was not subtracted). The solid line is the calculated profile. The tick marks below the profile indicate the position of allowed Bragg reflections. A difference plot (observed minus calculated) is plotted at the bottom. In the $\lambda_1 = 1.594$ Å pattern, a narrow region near $2\theta = 150°$ was excluded due to the presence of an aluminum peak from the cryostat tail.

$La_{0.75}Ca_{0.25}MnO_3$ at 20 K are shown in Fig. 1. For ferromagnetic samples of the $A_{0.7}A'_{0.3}MnO_3$ series, a simple model with collinear Mn moments, which were refined, was sufficient to describe the magnetic scattering at the present instrumental resolution. One sample of the series, with composition $Pr_{0.7}Ca_{0.3}MnO_3$, displayed a very complex magnetic structure, with the coexistence of both ferromagnetism and antiferromagnetism. The antiferromagnetic component of this structure contains two propagation vectors (1/2 00 and 1/2 0 1/2), associated with two Mn sublattices.[24] A ferromagnetic (FM) moment of 0.48(2) was also refined for the Pr site, but the small improvement of the R value is not considered sufficient proof of the Pr magnetic ordering. For the $La_{0.75}Ca_{0.25}MnO_3$ sample, due to the higher resolution configuration employed for the neutron data collection, significantly better refinements could be obtained with the Mn spins parallel to the c axis, with respect to the two other orientations. The structural parameters of the $A_{0.7}A'_{0.3}MnO_3$ compounds at 300 and 1.6 K, for the three space-group symmetries encountered in the system (Pnma, $R\bar{3}c$, and Imma) are listed in Tables I, II, and III, respectively. The $La_{0.75}Ca_{0.25}MnO_3$ structural parameters at selected temperatures are reported in Table IV.

III. METAL-INSULATOR TRANSITION AS A FUNCTION OF TEMPERATURE

As already discussed in Ref. 4, the lattice parameters and unit-cell volume of $La_{0.75}Ca_{0.25}MnO_3$ display a sharp discontinuity at $T_C = 240$ K. The lattice parameters as determined from neutron powder-diffraction data are consistent with the previous synchrotron x-ray-diffraction determination, and will not be reported herein. Here, we focus on the behavior of the *internal* structural parameters (bond distances and angles and Debye-Waller factors) as a function of temperature. Figure 2 shows the three crystallographically independent Mn-O bond lengths (center panel) and their average value ⟨Mn-O⟩ (top panel) as a function of temperature, evidencing the presence of a discontinuity at T_C for all parameters. In particular, the abrupt reduction of ⟨Mn-O⟩ at T_C is consistent with the formation of stronger metallic bonds in the ferromagnetic phase, and is the parameter which is pri-

TABLE I. Refined structural parameters from neutron powder-diffraction data for the $A_{0.7}A'_{0.3}MnO_3$ compounds having Pnma (No. 62) space-group symmetry. Numbers in parentheses are statistical errors of the last significant digit. The site occupancies are kept at fixed values consistent with the nominal stoichiometry. The atomic positions are Mn: 4*b* 1 (0,0,0.5); *A*/*A*′, O(1): 4*c* .*m*. (*x*,0.25,*z*), O2: 8*d* 1 (*x*,*y*,*z*). The low-temperature magnetic structure of $Pr_{0.7}Ca_{0.3}MnO_3$ has a ferromagnetic (FM) and an antiferromagnetic (AFM) component (Ref. 24). A FM moment of 0.48(2) was also refined for the Pr site.

A/*A*′ Site		$Pr_{0.7}Ca_{0.3}$		$La_{0.525}Pr_{0.175}Ca_{0.3}$		$La_{0.7}Ca_{0.17}Sr_{0.13}$		$La_{0.7}Ca_{0.13}Sr_{0.17}$
Temperature		300 K	1.6 K	300 K	1.6 K	300 K	1.6 K	1.6 K
a	(Å)	5.4646(2)	5.4663(2)	5.4585(2)	5.4493(1)	5.4690(1)	5.4563(1)	5.4572(1)
b	(Å)	7.6749(3)	7.6659(3)	7.7146(2)	7.6987(2)	7.7292(2)	7.7129(2)	7.7145(2)
c	(Å)	5.4308(2)	5.4240(2)	5.4674(2)	5.4579(1)	5.5045(1)	5.4901(1)	5.4968(1)
V	($Å^3$)	227.77(2)	227.17(2)	230.23(1)	228.97(1)	232.679(9)	231.046(8)	231.409(8)
μ	(μ_B)	0	FM 2.13(2) AFM 1.42(2)	0	3.43(3)	2.08(3)	3.46(3)	3.51(3)
Mn	u_{iso} ($Å^2$)	0.0026(4)	0.0026(4)	0.0028(4)	0.0018(4)	0.0043(4)	0.0012(4)	0.0007(4)
A/*A*′	*x*	0.0354(4)	0.0383(4)	0.0236(4)	0.0248(3)	0.0117(4)	0.0147(3)	0.0115(3)
	z	−0.0055(7)	−0.0031(7)	−0.0057(7)	−0.0045(5)	−0.0028(3)	−0.0032(2)	−0.0027(2)
	u_{iso} ($Å^2$)	0.0087(4)	0.0064(4)	0.0079(4)	0.0031(3)	0.0077(3)	0.0030(3)	0.0025(3)
O(1)	*x*	0.4853(4)	0.4844(4)	0.4893(7)	0.4905(5)	0.4944(6)	0.4947(4)	0.4963(5)
	z	0.0719(4)	0.0731(4)	0.0668(5)	0.0655(4)	0.0587(3)	0.0581(3)	0.0570(3)
	u_{11} ($Å^2$)	0.020(1)	0.022(1)	0.018(2)	0.005(2)	0.013(1)	0.010(1)	0.008(1)
	u_{22} ($Å^2$)	0.006(1)	0.001(1)	0.005(2)	0.003(1)	0.005(1)	0.005(1)	0.005(1)
	u_{33} ($Å^2$)	0.007(1)	0.005(1)	0.005(2)	0.003(1)	0.007(1)	0.0088(9)	0.008(1)
	u_{13} ($Å^2$)	−0.0039(9)	0.003(1)	−0.002(1)	−0.0005(9)	0.000(1)	0.0002(9)	0.001(1)
O(2)	*x*	0.2878(3)	0.2898(3)	0.2782(5)	0.2789(4)	0.2672(3)	0.2692(2)	0.2658(3)
	y	0.0374(2)	0.0380(2)	0.0342(2)	0.0338(2)	0.0306(2)	0.0309(1)	0.0301(1)
	z	0.7145(3)	0.7157(3)	0.7198(4)	0.7204(4)	0.7331(3)	0.7310(2)	0.7341(3)
	u_{11} ($Å^2$)	0.0177(7)	0.0192(7)	0.0104(8)	0.0033(6)	0.0121(8)	0.0044(7)	0.0036(7)
	u_{22} ($Å^2$)	0.0116(6)	0.0046(6)	0.0146(9)	0.0062(6)	0.0145(7)	0.0055(6)	0.0066(5)
	u_{33} ($Å^2$)	0.0111(6)	0.0081(6)	0.0156(9)	0.0062(7)	0.0130(7)	0.0057(6)	0.0075(6)
	u_{12} ($Å^2$)	−0.0014(5)	0.0009(6)	−0.001(1)	0.0004(8)	0.0025(9)	0.0009(7)	0.0015(8)
	u_{13} ($Å^2$)	−0.0019(6)	0.0011(6)	−0.0016(7)	−0.0010(5)	−0.0035(6)	−0.0022(5)	−0.0028(5)
	u_{23} ($Å^2$)	0.0015(6)	0.0007(6)	0.002(1)	0.0006(9)	0.0002(8)	0.0001(6)	0.0002(7)
R_{WP}	(%)	4.27	4.86	5.75	6.01	5.23	5.78	5.61
χ^2	(%)	1.581	2.534	1.660	1.809	1.729	2.033	1.753

marily responsible for the volume discontinuity. As already pointed out,[5] the behavior of the individual Mn-O bond lengths as a function of temperature is consistent with a reduction of the *coherent* JT distortion of the MnO_6 octahedra at T_C. However, it is necessary to stress that this coherent JT distortion is already very small *above* T_C. This can be quantified by defining a JT parameter

$$\sigma_{JT} = \sqrt{\frac{1}{3}\sum_i [(\text{Mn-O})_i - \langle \text{Mn-O} \rangle]^2},$$

(which is plotted as a function of temperature in Fig. 2, bottom panel). For $La_{0.75}Ca_{0.25}MnO_3$ at 300 K, $\sigma_{JT} \approx 3.7 \times 10^{-3}$, some 30 times smaller than for the prototype compound $LaMnO_3$ at the same temperature ($\sigma_{JT} = 1.2 \times 10^{-1}$).[32] Furthermore, for $La_{0.75}Ca_{0.25}MnO_3$, σ_{JT} *increases* with decreasing temperature below T_C and, at 20 K, becomes as large as at 300 K. Both these observations indicate that the behavior of the coherent JT distortion is a useful indication that a structural rearrangement is occurring at T_C, but cannot be taken as a conclusive proof of the role of lattice distortions in charge localization in the paramagnetic phase.

We should remark, however, that a small coherent JT distortion is not incompatible with a large total JT distortion, provided that the largest part of it cancels upon application of the space-group symmetry operators. This has been recently demonstrated in the case of the charge-ordered compound $La_{0.5}Ca_{0.5}MnO_3$ (Ref. 9). For $La_{0.5}Ca_{0.5}MnO_3$ at low temperatures, the Pnma-averaged JT distortion is very small [σ_{JT}(coherent) $= 1.9 \times 10^{-2}$] and of the *apically compressed* type (each Mn atom has two short and four long bonds with adjacent oxygen atoms). However, when the diffraction data are analyzed in terms of the quasicommensurate superstructure, the JT distortion of the $Mn^{3+}O_6$ octahedra is determined to be of the *apically elongated* type and to be as large as for $LaMnO_3$ [σ_{JT}(total) $= 1.2 \times 10^{-1}$]. Obviously, in this case, the Pnma-incoherent component of the JT distortion (i.e., the component which averages to zero upon application of the Pnma symmetry operators) is actually coherent with respect to the superstructure space group. If the diffraction data are analyzed using the Pnma space group, this Pnma-incoherent component is manifest only by rather large low-temperature oxygen Debye-Waller factors [$U(\text{O}) \sim 1 \times 10^{-2}$ as compared, for instance, to $U(\text{O}) \sim 3 \times 10^{-3}$ for $LaMnO_3$ at 2 K (Ref. 9)] indicating the presence of static disorder. In

TABLE II. Refined structural parameters from neutron powder-diffraction data for the $A_{1-x}A'_xMnO_3$ compounds having $R\bar{3}c$ (No. 167) space-group symmetry. The hexagonal axes setting was used for the refinement. Numbers in parentheses are statistical errors of the last significant digit. The site occupancies are kept at fixed values consistent with the nominal stoichiometry. The atomic positions are Mn: 6*b* $\bar{3}$. (0,0,0); *A*/*A*′: 6*a* 32 (0,0,0.25), O: 18*e* .2 (*x*,0,0.25).

A/*A*′ Site		$La_{0.7}Ca_{0.13}Sr_{0.17}$	$La_{0.7}Sr_{0.3}$		$La_{0.7}Ba_{0.18}Sr_{0.12}$	$La_{0.7}Ba_{0.3}$
Temperature		300 K	300 K	1.6 K	300 K	300 K
a	(Å)	5.5022(1)	5.5060(1)	5.499 30(9)	5.5245(1)	5.537 80(15)
c	(Å)	13.3291(3)	13.3564(3)	13.3175(3)	13.4431(3)	13.5011(4)
V	(Å^3)	349.47(1)	350.66(1)	348.80(1)	355.32(1)	358.57(2)
μ	(μ_B)	2.18(4)	2.36(4)	3.09(4)	2.29(4)	3.37(3)
Mn	u_{iso} (Å^2)	0.0053(5)	0.0037(5)	0.0024(5)	0.0036(5)	0.0038(6)
A/*A*′	u_{iso} (Å^2)	0.0075(3)	0.0072(3)	0.0040(3)	0.0076(3)	0.0094(4)
O	*x*	0.4515(1)	0.4577(1)	0.4563(1)	0.4647(1)	0.4706(2)
	u_{11} (Å^2)	0.0111(3)	0.0100(3)	0.0057(3)	0.0176(3)	0.0203(5)
	u_{22} (Å^2)	0.0099(5)	0.0086(5)	0.0047(4)	0.0133(5)	0.0135(7)
	u_{33} (Å^2)	0.0097(4)	0.0138(4)	0.0077(4)	0.0079(4)	0.0122(5)
	u_{12} (Å^2)	0.0050(2)	0.0043(2)	0.0023(2)	0.0066(3)	0.0067(3)
	u_{13} (Å^2)	−0.0014(2)	−0.0020(2)	−0.0014(2)	−0.0017(2)	−0.0023(3)
	u_{23} (Å^2)	0.0028(4)	0.0040(4)	0.0028(4)	0.0035(4)	0.0045(6)
R_{WP}	(%)	5.78	6.93	7.79	6.21	5.91
χ^2	(%)	2.262	2.461	3.038	3.780	3.244

TABLE III. Refined structural parameters from neutron powder-diffraction data for $A_{1-x}A'_xMnO_3$ compounds having Imma (No. 74) space-group symmetry. Numbers in parentheses are statistical errors of the last significant digit. The site occupancies are kept at fixed values consistent with the nominal stoichiometry. The atomic positions are Mn: 4*b* 2/*m*. (0,0,0.5); *A*/*A*′: 4*e* *mm*2 (0,0.25,*z*), O(1): 4*e* *mm*2 (0.5,0.25,*z*), O(2): 8*g* .2. (0.25,*y*,0.75).

A/*A*′ Site		$La_{0.7}Ba_{0.18}Sr_{0.12}$	$La_{0.7}Ba_{0.3}$
Temperature		1.6 K	1.6 K
a	(Å)	5.4903(1)	5.508 88(8)
b	(Å)	7.7607(2)	7.788 2(1)
c	(Å)	5.5295(1)	5.539 56(8)
V	(Å^3)	235.603(8)	237.669(6)
μ	(μ_B)	3.40(3)	3.37(3)
Mn	u_{iso} (Å^2)	0.0012(3)	0.002 2(5)
A/*A*′	*z*	0.0019(2)	0.001 8(3)
	u_{iso} (Å^2)	0.0023(2)	0.003 0(3)
O(1)	*z*	0.0451(3)	0.039 1(4)
	u_{11} (Å^2)	0.008(1)	0.011(2)
	u_{22} (Å^2)	0.004(8)	0.004(1)
	u_{33} (Å^2)	0.0110(7)	0.015(1)
O(2)	*y*	0.0225(1)	0.019 5(2)
	u_{11} (Å^2)	0.0038(7)	0.007(1)
	u_{22} (Å^2)	0.0132(5)	0.013 7(7)
	u_{33} (Å^2)	0.0106(5)	0.013 9(7)
	u_{13} (Å^2)	−0.0030(5)	−0.005 3(7)
R_{WP}	(%)	5.05	5.43
χ^2	(%)	2.568	2.651

the case of the paramagnetic phase of $La_{0.75}Ca_{0.25}MnO_3$ and other near optimally doped compositions, the absence of charge ordering indicates that, if present, the residual JT distortion must be truly incoherent, either through static or dynamic disorder.

The temperature dependence of the anisotropic oxygen Debye-Waller factors for $La_{0.75}Ca_{0.25}MnO_3$ is plotted in Fig. 3. We have chosen to plot $\langle U \rangle$ (defined as 1/3 the trace of the Debye-Waller tensor), and the projections of the thermal ellipsoid along the directions of the Mn-O bonds (U_{par}) and on the plane perpendicular to them (U_{perp}). U_{perp} is always *larger* than (U_{par}), as phonon energies are lower for tilting modes than for breathing modes. However, U_{par} displays a rather flat temperature dependence above T_C, and a sharp drop at T_C, while U_{perp} has a linear temperature dependence above T_C and a much smaller discontinuity. These data are consistent with the presence, above T_C, of incoherent structural distortions which involve oxygen displacements, mainly along the Mn-O bonds. Furthermore, the absolute value of U_{par} at $T_C(\sim 1\times 10^{-2}$ Å$^2)$ implies a mean-squared displacement of the oxygen atoms of ~ 0.1 Å, which is comparable with σ_{JT} for $LaMnO_3$ or the $La_{0.5}Ca_{0.5}MnO_3$ superstructure. All these observations support the possibility that, in the paramagnetic phase, the $Mn^{3+}O_6$ octahedra may be nearly *fully distorted*, the largest part of this distortion being incoherent. Our results are also in good agreement with the evidence obtained using probes that are sensitive to the local structure, like neutron-scattering pair-distribution-function analysis[20] and extended x-ray-absorption fine structure.[33]

Figure 4 shows the Mn-O-Mn bond angles as a function of temperature for $La_{0.75}Ca_{0.25}MnO_3$. This parameter is important because it is related to the electronic bandwidth, as discussed in Sec. V. Both crystallographically independent Mn-O-Mn angles suddenly increase at T_C. This fact, along

TABLE IV. Refined structural parameters from neutron powder-diffraction data for $La_{0.75}Ca_{0.25}MnO_3$ at selected temperatures. The space group symmetry is Pnma (No. 62). Numbers in parentheses are statistical errors of the last significant digit. The site occupancies are kept at fixed values consistent with the nominal stoichiometry. The atomic positions are Mn: 4*b* 1 (0,0,0.5); La/Ca, O(1): 4*c* .*m*. (*x*,0.25,*z*), O(2): 8*d* 1 (*x*,*y*,*z*).

Temperature		20 K	130 K	220 K	240 K	250 K	300 K	360 K	420 K
a	(Å)	5.470 57(3)	5.472 31(3)	5.476 94(4)	5.480 41(4)	5.480 51(4)	5.481 84(4)	5.483 77(4)	5.485 74(4)
b	(Å)	7.733 74(4)	7.736 84(4)	7.743 65(6)	7.747 60(6)	7.748 02(5)	7.751 50(5)	7.755 73(5)	7.759 80(5)
c	(Å)	5.488 53(3)	5.490 75(3)	5.494 96(4)	5.496 65(4)	5.496 95(4)	5.499 64(4)	5.503 09(4)	5.506 54(4)
V	($Å^3$)	232.208(2)	232.470(2)	233.050(3)	233.389(3)	233.417(3)	233.694(3)	234.050(3)	234.404(3)
μ_z	(μ_B)	3.51(1)	3.33(1)	2.29(1)	0.07(3)	0	0	0	0
Mn	u_{iso} ($Å^2$)	0.000 3(2)	0.001 3(2)	0.002 1(2)	0.0027(2)	0.002 3(2)	0.002 9(2)	0.003 6(2)	0.004 3(2)
La/Ca	*x*	0.021 3(1)	0.020 9(1)	0.021 0(1)	0.021 4(1)	0.021 5(1)	0.020 8(1)	0.019 9(1)	0.018 8(1)
	z	−0.004 3(1)	−0.004 4(1)	−0.004 1(2)	−0.004 4(2)	−0.004 4(2)	−0.004 3(2)	−0.004 1(2)	−0.003 9(1)
	u_{iso} ($Å^2$)	0.002 3(1)	0.003 6(1)	0.005 8(1)	0.007 1(1)	0.006 9(1)	0.007 5(1)	0.008 6(1)	0.009 9(1)
O(1)	*x*	0.491 8(2)	0.491 6(2)	0.492 0(2)	0.491 2(2)	0.491 3(2)	0.491 4(2)	0.491 8(2)	0.492 3(2)
	z	0.064 0(1)	0.064 1(1)	0.064 7(1)	0.065 0(2)	0.065 1(1)	0.064 7(1)	0.064 4(1)	0.063 8(1)
	u_{11} ($Å^2$)	0.006 3(5)	0.007 8(5)	0.012 1(6)	0.013 6(6)	0.013 5(6)	0.015 2(6)	0.015 7(6)	0.018 0(6)
	u_{22} ($Å^2$)	0.001 2(4)	0.002 7(4)	0.005 5(5)	0.008 3(5)	0.007 5(5)	0.007 7(5)	0.008 3(5)	0.009 0(5)
	u_{33} ($Å^2$)	0.003 1(3)	0.004 1(4)	0.004 9(4)	0.007 3(4)	0.006 9(4)	0.008 1(4)	0.010 0(4)	0.011 5(4)
	u_{13} ($Å^2$)	0.000 4(3)	0.000 3(3)	−0.000 7(4)	−0.000 5(4)	−0.000 92(4)	−0.000 7(4)	−0.000 8(4)	−0.001 5(4)
O(2)	*x*	0.276 0(1)	0.275 8(1)	0.276 0(1)	0.277 1(1)	0.277 3(1)	0.276 7(1)	0.276 0(1)	0.275 3(1)
	y	0.033 23(6)	0.033 20(7)	0.033 25(8)	0.033 73(8)	0.033 6(8)	0.033 37(8)	0.033 10(8)	0.032 88(8)
	z	0.725 43(9)	0.725 54(9)	0.724 50(1)	0.724 3(1)	0.724 3(1)	0.724 6(1)	0.725 2(1)	0.725 8(1)
	u_{11} ($Å^2$)	0.003 5(2)	0.004 8(2)	0.008 2(3)	0.009 5(3)	0.009 4(3)	0.010 2(3)	0.011 3(3)	0.012 9(3)
	u_{22} ($Å^2$)	0.003 9(2)	0.005 5(2)	0.009 1(3)	0.010 2(3)	0.010 4(3)	0.011 4(3)	0.013 3(3)	0.014 3(3)
	u_{33} ($Å^2$)	0.003 2(2)	0.004 4(2)	0.006 0(3)	0.009 7(3)	0.009 6(3)	0.010 3(3)	0.011 4(3)	0.012 3(3)
	u_{12} ($Å^2$)	0.000 06(3)	0.000 1(3)	0.000 3(3)	0.000 63(3)	0.000 3(3)	0.000 2(3)	−0.000 2(3)	−0.000 5(3)
	u_{13} ($Å^2$)	−0.000 9(2)	−0.001 2(2)	−0.000 9(2)	−0.000 5(2)	−0.000 9(2)	−0.001 7(2)	−0.001 7(2)	−0.002 5(3)
	u_{23} ($Å^2$)	0.000 7(3)	−0.000 5(3)	−0.000 8(2)	−0.000 1(4)	0.000 5(3)	−0.000 4(3)	−0.000 4(3)	0.000 2(4)
R_{WP}	(%)	4.34	4.32	4.34	4.27	4.04	3.89	3.76	3.64
χ^2	(%)	2.99	2.94	3.00	2.95	2.69	2.51	2.30	2.21

with the concurrent drop of ⟨Mn-O⟩, is consistent with a large value of the bandwidth *W* in the metallic phase. It is noteworthy that the behaviors of ⟨Mn-O⟩ and of ⟨Mn-O-Mn⟩ have opposite effects on the unit-cell volume, which for a distorted perovskite, can be expressed as

$$V \approx Z[2\langle \text{Mn-O}\rangle \cos\omega]^3, \tag{3.1}$$

where

$$\omega = \frac{1}{2}\,(\pi\text{-}\langle \text{Mn-O-Mn}\rangle), \tag{3.2}$$

and *Z* is the number of formula units in the unit cell ($Z=4$ for the present case). The volume *increase* at T_C on cooling, produced by the sudden increase of ⟨Mn-O-Mn⟩, is overcompensated by a volume decrease due to the ⟨Mn-O⟩ drop, yielding the observed volume contraction.

IV. METAL-INSULATOR TRANSITION AS A FUNCTION OF $\langle r_A \rangle$

A considerable amount of work has been recently devoted to the evolution of the transport and magnetic properties by altering, at constant electronic doping, the ionic radii of the *A*-site ions. Usually, the evolution of the physical properties is described in terms of the average *A*-site ionic radius $\langle r_A \rangle$. We should stress that $\langle r_A \rangle$ has simply the meaning of a continuous abscissa used to plot physical or structural parameters. In fact, the ''true'' ionic radius is a rather ill-defined concept, since it depends on the *A*-site coordination, which, as we shall see, is itself a function of $\langle r_A \rangle$. Therefore, for the present and previous[1,5,6] papers, in order to avoid complications, we chose to calculate ionic radii at constant coordination number (9), using tabulated values.[31] The choice of ninefold coordination was made simply because this is the highest coordination number for which tabulated data are available for all the cations of our series. The parameter $\langle r_A \rangle$ can be continuously varied only by making solid solutions with variable concentrations of ions of different sizes, and, to this end, for each $\langle r_A \rangle$, several combinations of large and small ions may be used. A recent work by Rodriguez-Martinez and Attfield[34] has indicated that samples with equal $\langle r_A \rangle$ and doping level *x* may have different properties, depending on whether ions with widely different radii (e.g., Lu and Ba) or almost equal radii (e.g., Pr and Ca) are used. In other words, in addition to *x* and $\langle r_A \rangle$, the cation-size disorder parameter, $\sigma(r_A)$, may also play a role. The magnetic properties of the rare-earth ions may also be important, especially at low temperatures. In the present paper, keeping in mind these *caveats*, we will nonetheless follow the ''traditional'' approach of using *x* and $\langle r_A \rangle$ as the only ''chemical'' parameters (the possible effects of $\sigma(r_A)$ upon the elec-

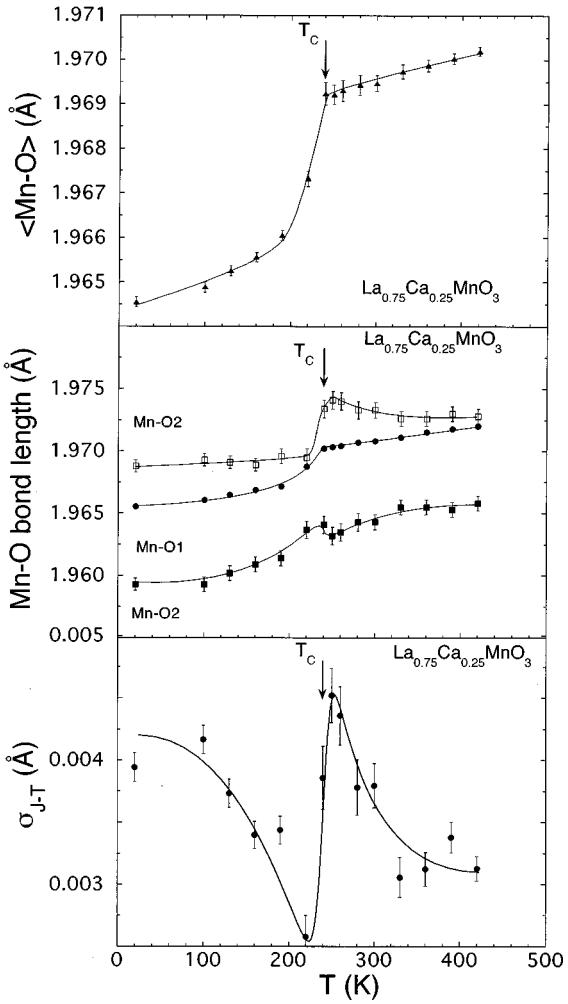

FIG. 2. Effects of the magnetic and metal-insulator transition on the Mn-O bond lengths for $La_{0.75}Ca_{0.25}MnO_3$. Average Mn-O bond length: (top), individual Mn-O bond lengths (center) and Jahn-Teller distortion parameter $\sigma_{JT}=\sqrt{1/3\,\Sigma_i[(\text{Mn-O})_i-\langle\text{Mn-O}\rangle]^2}$ (bottom). The arrows indicate the position of the magnetic and metal-insulator transition.

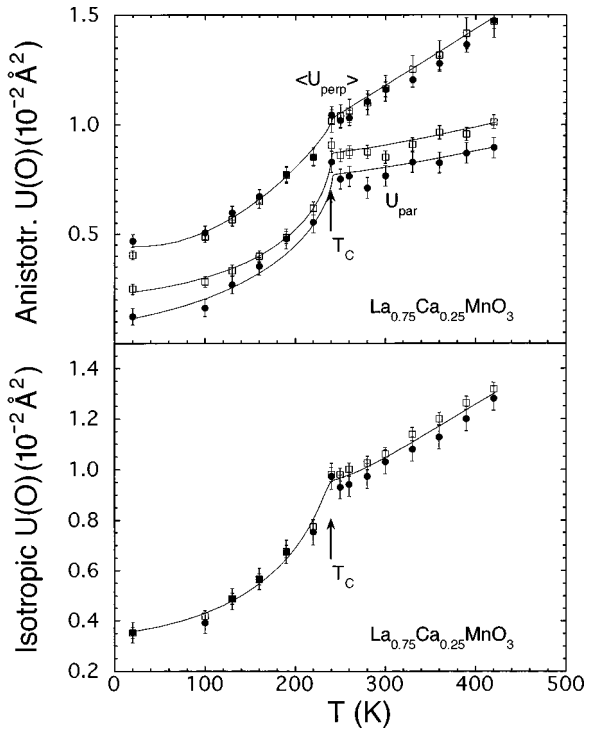

FIG. 3. Incoherent distortions of the MnO_6 octahedra vs temperature for $La_{0.75}Ca_{0.25}MnO_3$. Isotropic oxygen Debye-Waller factor, defined as 1/3 of the trace of the Debye-Waller tensor, (bottom), and projections of the oxygen anisotropic Debye-Waller factors *parallel* (U_{par}) and *perpendicular* ($\langle U_{perp}\rangle$) (top) to the direction of the Mn-O bond lengths for O(1) (filled circles) and O(2) (open squares).

tronic bandwidth W and the JT localization energy E_{JT} will be discussed in Sec. V). We remark, however, that, due to the choice of metal ions used to synthesize our series, there is a systematic *increase* of $\sigma(r_A)$ as a function of $\langle r_A\rangle$, from 4.58×10^{-4} for $Pr_{0.7}Ca_{0.3}MnO_3$ ($\langle r_A\rangle=1.179$) to 1.16×10^{-1} for $La_{0.7}Ba_{0.3}MnO_3$ ($\langle r_A\rangle=1.292$). In the present section we focus on the structural effects occurring at the metal-insulator transition as a function of $\langle r_A\rangle$, while Sec. V is be devoted to the changes of the electronic bandwidth W induced by varying $\langle r_A\rangle$ (''chemical'' pressure) and by applying an external pressure.

It has previously been shown that, for a constant $x=0.3$ value, the low-temperature transport and magnetic properties of $A_{1-x}A'_xMnO_3$ change from canted antiferromagnetic insulator (CAF) for small $\langle r_A\rangle$ to ferromagnetic metal (FM) for large $\langle r_A\rangle$. Furthermore, the Curie temperature is a nonmonotonic function of $\langle r_A\rangle$, reaching a maximum for the composition $La_{1-x}Sr_xMnO_3$ ($\langle r_A\rangle\approx1.24$ Å). Inspection of the T vs $\langle r_A\rangle$ phase diagram[1] indicates that two types of M-I transitions occur: from CAF to FM (at low temperatures) and from the paramagnetic insulator (PI) phase to FM around room temperature (the radii at these M-I transitions $r_{M\text{-}I}$, being 1.185 and 1.216 Å at 2 and 293 K, respectively). The $A_{1-x}A'_xMnO_3$ structural phase diagram has also been previously reported.[6] Three allotypes of the perovskite structure (with space groups Pnma, $R3c$, and Imma) have been shown to exist in this range of parameters. In this section, we focus on the variation of the structural properties as a function of $\langle r_A\rangle$ relating to the M-I transitions.

The Mn-O bond lengths and the average oxygen Debye-

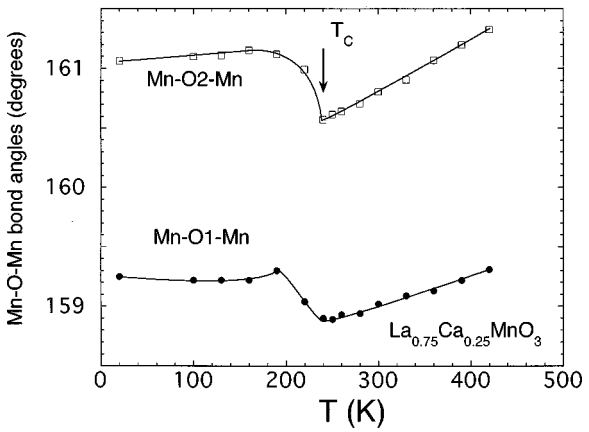

FIG. 4. Mn-O-Mn bond angles as a function of temperature for $La_{0.75}Ca_{0.25}MnO_3$. The error bars are smaller than the symbols. Lines are guides to the eye.

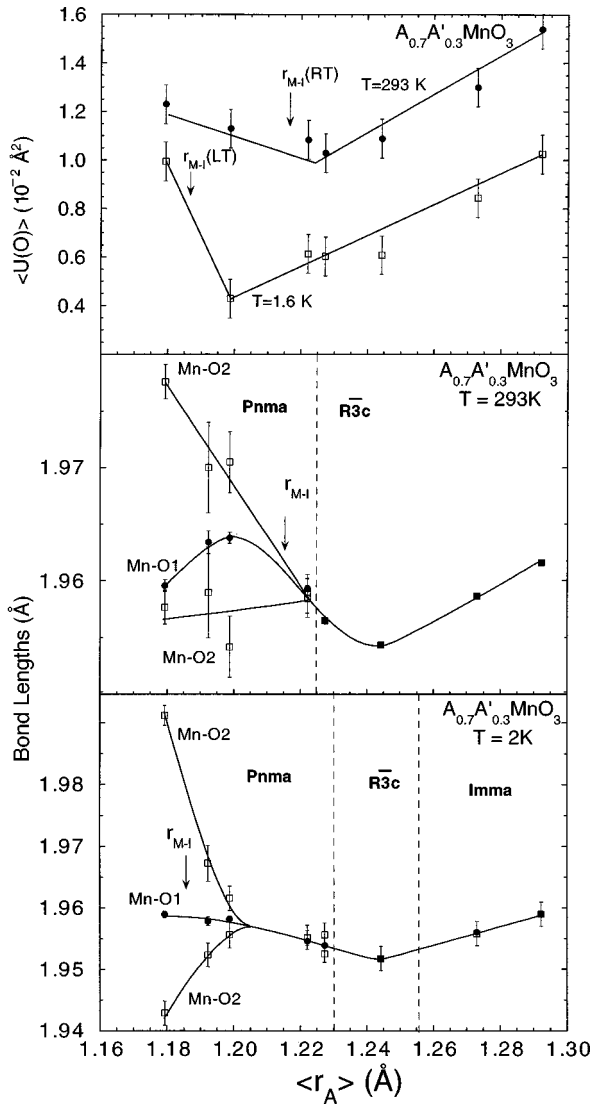

FIG. 5. Coherent distortion of the MnO_6 octahedra as a function of $\langle r_A \rangle$ for $A_{0.7}A'_{0.3}MnO_3$ (see also Ref. 5). Mn-O bond lengths at 2 K (lower) and 293 K (center), and average oxygen Debye-Waller factors (top). The dashed lines separate the different structural phases. Error bars are either shown or smaller than the symbols. Solid lines are guides to the eyes.

Waller factor (defined as 1/3 the trace of the Debye-Waller tensor in the orthorhombic phases, the average over the two independent oxygen sites is also performed), as a function of $\langle r_A \rangle$ are shown in Fig. 5 for $T=293$ and 2 K. For $Pr_{0.7}Ca_{0.3}MnO_3$, which is the sample of our series having the smallest $\langle r_A \rangle$ value, both the coherent JT distortion and the oxygen Debye-Waller factors are rather large: $\sigma_{JT}=2.0\times10^{-2}$ and 7.7×10^{-3}, and $U(O)=1.2\times10^{-2}$ and 1.0×10^{-2} at 2 and 293 K, respectively. With increasing $\langle r_A \rangle$, the coherent JT distortion decreases and finally disappears above $r_{M\text{-}I}$. It should be pointed out that, as in the previously discussed $La_{0.75}Ca_{0.25}MnO_3$ case, a few samples in the FM phase have a small but still measurable value of σ_{JT} at low temperatures. The oxygen Debye-Waller factors $U(O)$ show a similar albeit slightly more complex behavior. The abrupt reduction of $U(O)$ in the vicinity of $r_{M\text{-}I}$ is evident, especially in the low-temperature data. It is noteworthy, however that this behavior is superimposed on an *increase* of $U(O)$ as a function of $\langle r_A \rangle$. The likely cause of this effect is the aforementioned systematic increase of $\sigma(r_A)$ as a function of $\langle r_A \rangle$, which induces structural disorder in the position of the oxygen atoms, which are coordinated with the *A*-site cations. This disorder manifests itself as a temperature-independent contribution to the oxygen Debye-Waller factors.

The behavior of the Mn-O distances and of $U(O)$ just described is consistent with the picture we have established for $La_{0.75}Ca_{0.25}MnO_3$: the metallic phase (above $r_{M\text{-}I}$) is characterized by a small coherent JT distortion of the MnO_6 octahedra and by small $U(O)$'s, whereas, in the insulating phases, these parameters are larger. Furthermore, if the large $U(O)$'s are interpreted as arising from an incoherent JT distortion of the MnO_6 octahedra, the total JT distortions of the $Mn^{3+}O_6$ octahedra can be as large as in $LaMnO_3$ (note that, in the ideal case of complete charge localization, only 70% of the MnO_6 octahedra are expected to be Jahn-Teller distorted, since the formal valence of Mn in $A_{0.7}A'_{0.3}MnO_3$ is 3.3). What is particularly noteworthy about the $A_{1-x}A'_xMnO_3$ series is the existence of similarities between the average structures of the PI phase (all RT samples below $r_{M\text{-}I}$) and of the CAF phase ($Pr_{0.7}Ca_{0.3}MnO_3$ at 2 K), in that both support large (coherent and incoherent) JT distortions. These similarities will be discussed in further detail in Sec. VI.

V. EFFECTS OF ''CHEMICAL'' AND APPLIED PRESSURE

As already mentioned, the magnetic and transport properties can be varied at constant doping by varying the *A*-site cation composition[1,7,8,34] or by applying external pressure.[2,28,29] A metal-insulator transition can be induced by decreasing the average *A*-site ionic radius $\langle r_A \rangle$ below a critical value ($\langle r_A \rangle \approx 1.18$). In the metallic regime, T_C varies by more than a factor of 2 as a function of $\langle r_A \rangle$, and, for the Mn^{4+}/Mn^{3+} ratio of 0.3, it displays a maximum corresponding to the composition $La_{0.7}Sr_{0.3}MnO_3$ ($\langle r_A \rangle = 1.244$). The application of external pressure always increases T_C, with dT_C/dP varying in the range $5-50$ K GPa^{-1}. These effects have been discussed by the majority of authors in terms of a variation of the electronic bandwidth *W* as a function of chemical and applied pressure, with the main focus being on the influence of the Mn-O-Mn bond angle on *W*. Mn-O-Mn is expected to increase both as a function of increasing $\langle r_A \rangle$ and as a function of applied pressure, which would account for the general trend of increasing T_C with these parameters (the metallic phase is stabilized by larger values of *W*). According to the most recent theoretical discussions, it appears that, in addition to *W*, another energy scale acts as an essential ingredient in the description of these systems, namely the JT energy E_{JT}. For instance, Millis, Shraiman, and Mueller[18] have proposed a generalized phase diagram of the manganites at constant doping $x\sim0.3$, as a function of the reduced temperature T/t (t is the electron hopping parameter, which is proportional to *W*), and of the electron-phonon coupling $\lambda = E_{JT}/t$. As a consequence, possible variations of E_{JT} as a function of ''chemical'' or applied pressure need to be taken into consideration. This approach was recently followed by

Rodriguez-Martinez and Attfield,[34] in their description of the effects on T_C of varying the cation size disorder at constant x and $\langle r_A \rangle$. Rodriguez-Martinez and Attfield note that T_C is strongly suppressed when mixtures of very large and very small cations are used, and interpret this effect by hypothesizing that the strain field induced by the cation size disorder stabilizes the JT distortions, effectively increasing the parameter E_{JT}. It has to be noted, however, that the lattice parameters reported by Rodriquez-Martinez and Attfield indicate significant changes in the average structure, and, in particular, an increase of the unit-cell volume by 0.5% throughout the series. Since no information on the internal structural parameters is available for this series of samples, it is impossible to ascertain whether the observed T_C variation is due to an increase of E_{JT}, as proposed by the authors, or to a reduction of W, which could be a consequence of an increase of the average Mn-O bond length (see below). In the remainder of this section, we present a detailed study of the evolution of the internal structural parameters as a function of $\langle r_A \rangle$ and applied pressure for our samples. Based on these data, we estimate the corresponding changes in W. Our data indicate that all the observed T_C variations can be explained, at least qualitatively, by changes of the W parameter, but do not completely rule out a contribution from a variation of E_{JT}, which is, however, much more difficult to estimate (some qualitative considerations are presented at the end of this section). Our results also indicate that, in addition to the Mn-O-Mn bond angle, Mn-O bond distance changes play a major role in influencing W, especially as a function of applied pressure. These conclusions are based on the evolution of the structural parameters (bond lengths and angles) *averaged* over the crystallographically independent values. This procedure is always justified for the Mn-O-Mn bond angles, since the difference between Mn-O1-Mn and Mn-O2-Mn in the orthorhombic phases is only 1–3°. As far as the Mn-O bond lengths are concerned, some *caveats* are necessary, since, as we have seen, a measurable coherent JT distortion is present in the paramagnetic phase at low $\langle r_A \rangle$.

For perovskite compounds with general formula ABX_3, it is a straightforward result from tight-binding approximation that W depends on both the B-X-B bond angles and B-X bond lengths, through the overlap integrals between the $3d$ orbitals of the metal ion B and the $2p$ orbitals of the X anion. The following empirical formula has been used to describe this double dependence:[35]

$$W \propto \frac{\cos\omega}{d_{B\text{-}X}^{3.5}}, \tag{5.1}$$

where ω is the ''tilt'' angle in the plane of the bond [already defined in Eq. (3.2)], and is given by $\omega = \frac{1}{2}(\pi - \langle B\text{-}X\text{-}B \rangle)$, and $d_{B\text{-}X}$ is the B-X bond length. From the previous formulas it is clear that, for weakly distorted structures like the manganite perovskites, where cos ω is close to 1, only very large changes in the B-X-B bond angle can significantly affect W. The *average* Mn-O bond lengths and Mn-O-Mn bond angles as a function of $\langle r_A \rangle$ for our series of samples are plotted in Fig. 6 (bottom and top panels, respectively). The change of the Mn-O-Mn bond angles is apparently quite remarkable (14° throughout the range). However, the total change in cos ω is very small, less than 2% and is comparable to the

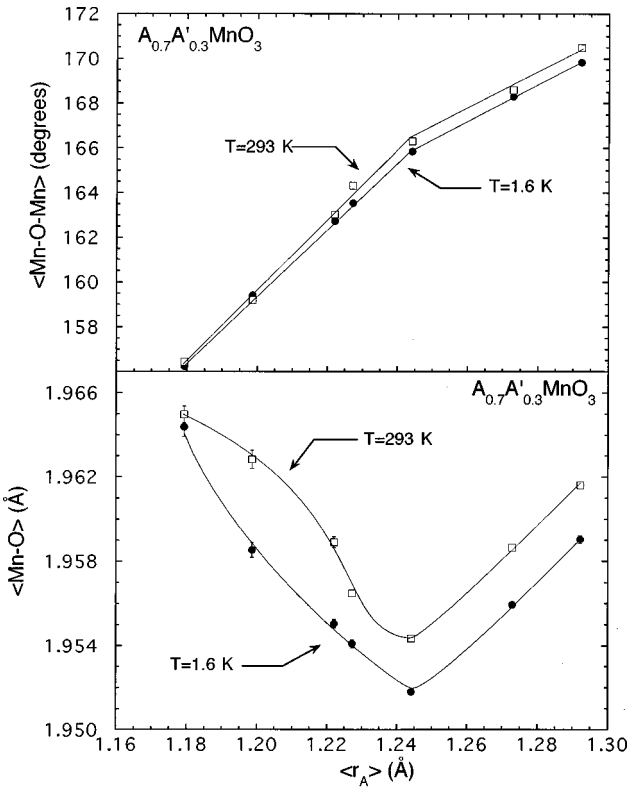

FIG. 6. Structural parameters affecting the electronic bandwidth W: average Mn-O bond lengths (bottom) and Mn-O-Mn bond angles (top) as a function of $\langle r_A \rangle$ for $A_{0.7}A'_{0.3}MnO_3$.

$\langle$Mn-O$\rangle$ change (about 1%), as shown in Fig. 7 (bottom panel). Therefore, the presence of a *minimum* in $\langle$Mn-O$\rangle$ for $\langle r_A \rangle \sim 1.24$ has remarkable consequences on the evolution of $[\cos\omega/d_{B\text{-}X}^{3.5}]$ [assumed to be proportional to W through Eq. (5.1)] as a function of $\langle r_A \rangle$ (Fig. 7, top panel). At low $\langle r_A \rangle$, the increase of $\langle$Mn-O-Mn$\rangle$ and the decrease of $\langle$Mn-O$\rangle$ both contribute to the rapid increase of W. At high $\langle r_A \rangle$, however, the two structural parameters have opposite effects on W, yielding a net *decrease* of W with a much smaller slope. The evolution of W as a function of $\langle r_A \rangle$ is remarkably similar to that of T_C. However, the conclusion that W is directly related to T_C, and, in particular, is solely responsible for the metal-insulator transition as a function of $\langle r_A \rangle$, should be taken with some care, as the total change of W throughout the metallic range is only about 4%, whereas T_C varies by more than a factor of 2. The bandwidth scenario, therefore, is plausible only assuming that T_C is very sensitive to small W variations. By comparison, in the generalized phase diagram proposed by Millis, Shraiman, and Mueller,[18] the E_{JT} parameter must vary by about 20% to obtain a comparable T_C variation.

The presence of a minimum in $\langle$Mn-O$\rangle$ (Fig. 6) is unexpected, and needs to be discussed. The minimum occurs within the trigonal phase, and cannot be correlated with the Pnma$\rightarrow R3c$ structural phase transition. On the other hand, chemical and iodometric analyses performed on the present and on similar samples rule out the possibility that the observed effect is due to a systematic change of the formal Mn valence throughout the series.[1] We propose that the presence of a minimum is due to the interplay between steric and

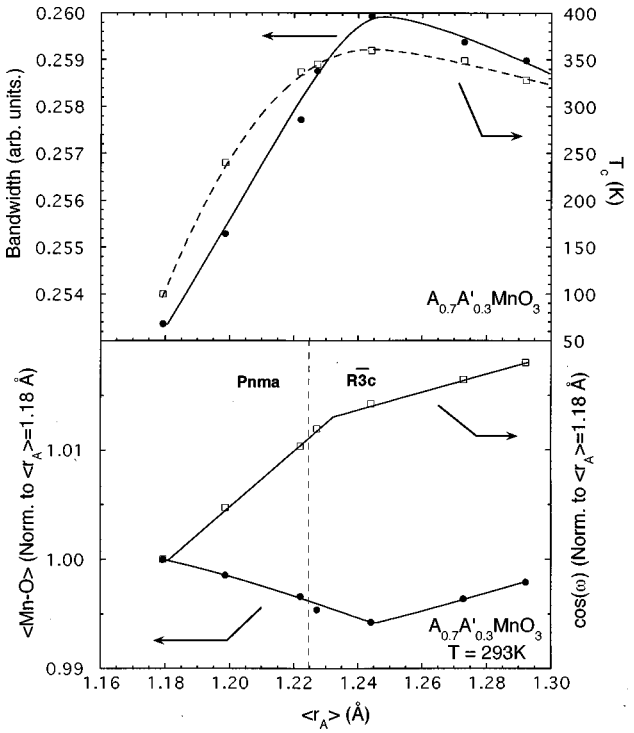

FIG. 7. Bottom: Relative changes of the average Mn-O bond lengths and cos ω [for the definition, see Eq. (3.2)] as a function of $\langle r_A \rangle$ normalized to the values for $Pr_{0.7}Ca_{0.3}MnO_3$ ($\langle r_A \rangle = 1.18$ Å). Top: comparison of the evolution of the cos $\omega/d_{B\text{-}X}^{3.5}$ ratio (assumed to be proportional to W, see Eq. (5.1) and of T_C as a function of $\langle r_A \rangle$.

coordination effects around the A site of the perovskite structure. At low values of $\langle r_A \rangle$, the octahedral framework folds around the small A-site cation until it attains equilibrium distances with 8 of the 12 surrounding oxygen atoms (eightfold coordination, see Fig. 8). The A-O distances with the three remaining oxygen atoms are in excess of 3 Å which makes them effectively nonbonded. In this situation, very little strain is imposed upon the Mn-O bond lengths, which can adjust to their optimal value. With increasing $\langle r_A \rangle$, the

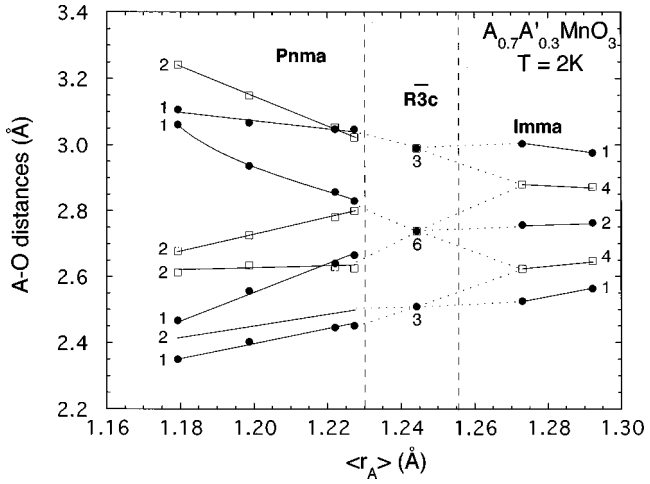

FIG. 8. A-site cation to oxygen bond lengths as a function of $\langle r_A \rangle$ at $T = 2$ K. The numbers beside the lines indicate the bond multiplicity in the various phases. Lines are guides to the eye.

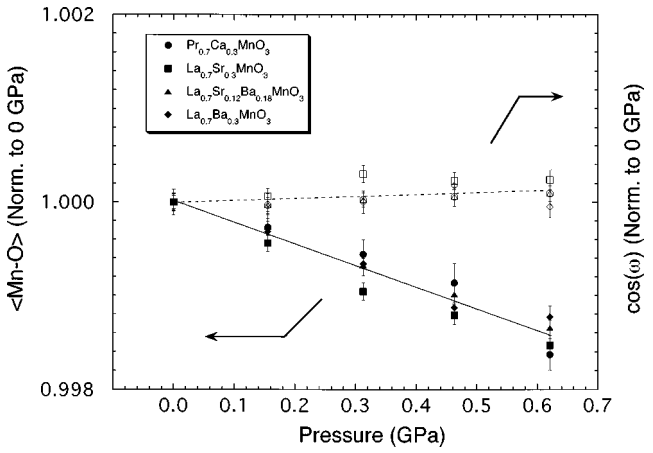

FIG. 9. Relative pressure evolution of the internal parameters, normalized as in Fig. 6, for selected samples of the $A_{0.7}A'_{0.3}MnO_3$ series. The right and left scales are identical. The lines are linear best fits through the average values between the different compositions.

octahedral framework untilts. As a consequence, the faraway oxygen atoms in the first coordination shell come closer to the A site, and start to feel an *attractive* interaction, which is transmitted to the Mn-O network as an effective ''internal'' pressure. For even larger values of $\langle r_A \rangle$, the A cations becomes effectively 12-fold coordinated, and the whole lattice, including the Mn-O distances, must expand with increasing $\langle r_A \rangle$. This reversal of the sign of the internal pressure could, in fact, be quite a general effect in perovskites, which deserves to be explored in other systems as well.

The application of an external pressure on these compounds produces quite different structural effects than the aforementioned ''internal'' pressure. The primary effect of the external pressure is to compress all the bond lengths (Mn-O and A-O). However, the A-O bonds are less compressible than the Mn-O bonds, whence a slight increase of the Mn-O-Mn bond angles as a function of pressure. We have measured the internal parameter compressibility for all the samples of our series up to ~ 0.6 GPa. No remarkable difference between the samples has been noted. Figure 9 shows the pressure evolution of the internal parameters, normalized as in Fig. 7. Although the behaviors of both $\langle$Mn-O$\rangle$ and cos ω go in the sense of an increase of W as a function of pressure, it is clear that $\langle$Mn-O$\rangle$ gives by far the largest contribution to this effect.

The determination of the relative compressibilities as a function of ''chemical'' and applied pressure allows an interesting quantitative comparison to be made between the their influence of T_C. Assuming that the internal structural parameters only influence T_C through W, that is, $T_C = T_C[W(d_{\text{Mn-O}}, \omega)]$, and using Eq. (5.1), one obtains

$$\frac{dT_C}{d\langle r_A \rangle} = W \frac{dT_C}{dW} [\kappa_\omega^r - 3.5\kappa_d^r], \tag{5.2}$$

$$\frac{dT_C}{dP} = W \frac{dT_C}{dW} [\kappa_\omega^P - 3.5\kappa_d^P], \tag{5.3}$$

where

$$\kappa_\omega^r = \frac{1}{\cos\omega}\frac{\partial\cos\omega}{\partial\langle r_A\rangle}; \quad \kappa_d^r = \frac{1}{\langle \text{Mn-O}\rangle}\frac{\partial\langle \text{Mn-O}\rangle}{\partial\langle r_A\rangle}, \quad (5.4)$$

$$\kappa_\omega^P = \frac{1}{\cos\omega}\frac{\partial\cos\omega}{\partial P}; \quad \kappa_d^P = \frac{1}{\langle \text{Mn-O}\rangle}\frac{\partial\langle \text{Mn-O}\rangle}{\partial P}, \quad (5.5)$$

are the ''internal'' and applied pressure compressibilities of the internal parameters. By taking the ratio between Eqs. (5.2) and (5.3), one obtains

$$\frac{dT_C/dP}{dT_C/d\langle r_A\rangle} = \frac{[\kappa_\omega^P - 3.5\kappa_d^P]}{[\kappa_\omega^r - 3.5\kappa_d^r]} = R_r^P, \quad (5.6)$$

where R_r^P is the radius-pressure conversion factor previously introduced in Ref. 2. In other words, it is possible to predict R_r^P purely based on *structural* parameters. The comparison with the experimental values obtained from transport property measurements can therefore be used to verify the bandwidth hypothesis.

The applied pressure compressibilities are easily evaluated from the fits in Fig. 9:

$$\kappa_\omega^P = 0.000\,21(7)\ \text{GPa}^{-1}; \quad \kappa_d^P = -0.002\,32(4)\ \text{GPa}^{-1}$$

and can be considered as independent of $\langle r_A\rangle$. The ''chemical'' pressure compressibilities obviously change as a function of $\langle r_A\rangle$, with κ_d^r notably changing sign. The following approximate values can be used:

$$\kappa_\omega^r = 0.23\ \text{Å}^{-1}; \quad \kappa_d^r = -0.11\ \text{Å}^{-1}$$

$$(\text{below } \langle r_A\rangle = 1.24\ \text{Å}),$$

$$\kappa_\omega^r = 0.08\ \text{Å}^{-1}; \quad \kappa_d^r = 0.08\ \text{Å}^{-1}$$

$$(\text{above } \langle r_A\rangle = 1.24\ \text{Å}).$$

From Eq. (5.6) we obtain

$$R_r^P = 0.0137\ \text{Å GPa}^{-1} \quad (\text{below } \langle r_A\rangle = 1.24\ \text{Å}),$$

$$R_R^P = -0.044\ \text{Å GPa}^{-1} \quad (\text{above } \langle r_A\rangle = 1.24\ \text{Å}).$$

These values are of the correct order of magnitude but are systematically larger than the experimental values, especially at high $\langle r_A\rangle$. For instance, for $\langle r_A\rangle = 1.205$ (corresponding to the composition $La_{0.7}Ca_{0.3}MnO_3$, studied in Ref. 2), based on an experimental value of $dT_C/d\langle r_A\rangle \approx 2700\ \text{K Å}^{-1}$, one would predict $dT_C/dP = 37$ K/GPa, to be compared with the experimental value $(dT_C/dP)_{\text{exp}} \approx 20$ K/GPa. In Ref. 2 we demonstrated that the effect of pressure could be mapped to changes in $\langle r_A\rangle$ for $\langle r_A\rangle \leqslant 1.24$ Å. However, above this value, our model predicts a *positive* dT_C/dP, although $dT_C/d\langle r_A\rangle$ is negative. In order to verify this, we have measured the pressure dependence of T_C for $La_{0.7}Ba_{0.3}MnO_3$ ($\langle r_A\rangle = 1.292$), and indeed found a *positive* dT_C/dP of ~ 6 K/GPa. This value is, however, smaller than the calculated value of 28 K/GPa, predicted on the basis of the experimental $dT_C/d\langle r_A\rangle \approx -630\ \text{K Å}^{-1}$. Obviously, the approximate nature of the bandwidth expression in Eq. (5.1) may explain some of this discrepancy. However, both the high values of $dT_C/d\langle r_A\rangle$ compared to dT_C/dP and the rather small total variation of W as a function of $\langle r_A\rangle$ suggest that at least part of the T_C variation with $\langle r_A\rangle$ may be attributed to a change in E_{JT}.

The changes in E_{JT} induced by varying the A-site cation composition are very difficult to estimate, and only qualitative considerations can be presented. E_{JT} is the difference between the on-site electronic energy, which is gained by distorting the ligand configuration around the Mn^{3+} ions, and the energy loss which results from the lattice distortions. The example of $La_{0.5}Ca_{0.5}MnO_3$ indicates that an optimal situation is realized by forming orbitally ordered configurations with very small net distortions,[9] which could also be present as short-range-ordered clusters in the PI phase (see Sec. VI). Although these JT distortions are expected to be largely incoherent, and therefore fairly insensitive to the global lattice symmetry, the A-site cation composition at constant doping could affect E_{JT} in at least two ways: (1) The eightfold coordination around the A site, which is observed for small values of $\langle r_A\rangle$ in the $Pnma$ phase, allows more flexibility than the higher coordinations encountered for large values of $\langle r_A\rangle$, three of the 12 oxygen atoms being effectively nonbonded. This means that fairly large (coherent and incoherent) fluctuations of the Mn-O bond length can be accommodated at little energy cost, effectively increasing E_{JT}. (2) As proposed by Rodriguez-Martinez and Attfield,[34] a similar effect could be induced by A-site size disorder (expressed in terms of the parameter $\sigma\langle r_A\rangle$), which would provide preferential sites to accommodate $Mn^{3+}O_6$ distorted octahedra. In summary, we conclude that the bandwidth scenario is able to explain, at least qualitatively, all the observed T_C variations as a function of ''chemical'' and applied pressure. However, a simultaneous influence of the JT energy E_{JT} cannot be ruled out, especially at very low $\langle r_A\rangle$ and at high $\sigma\langle r_A\rangle$. Clearly a more accurate description of the influence of the structural parameters upon the electronic structure of these materials is needed to clarify this issue.

VI. DISCUSSION AND CONCLUSIONS

In the previous sections we have discussed the structural properties of the three magnetotransport phases which are encountered for $x = 0.25$–0.30: paramagnetic insulator (PI) at high temperatures, charge-ordered spin-canted insulator (CAF) at low temperature and narrow bandwidth, and ferromagnetic metal (FM) at low temperature and wide bandwidth. We have shown that the average crystal structure is similar for the first two phases, and is characterized by large incoherent structural distortions of the JT type, which are accompanied, in the case of the $Pnma$ symmetry, by a measurable coherent JT effect. Both coherent and incoherent distortions are abruptly reduced by the transition into the ferromagnetic metal phase. We have also shown that the evolution of the electronic bandwidth, as determined from the internal structural parameters, is sufficient to explain, at least qualitatively, the evolution of T_C as a function of ''chemical'' and applied pressure in the metallic phase as well as the presence of a metal-insulator transition at narrow bandwidths as a function of $\langle r_A\rangle$. However, the similarities between the average structures of the charge-ordered and paramagnetic phases deserve to be discussed in further de-

tail. To understand this relationship, it is useful to point out that a phase transition between the charge-ordered and paramagnetic phases occurs as a function of temperature for narrow-bandwidth compositions. This phase transition has been studied, for instance, by De Teresa *et al.*,[36] using dilatometric techniques for the composition $Pr_{2/3}Ca_{1/3}MnO_3$. This study has evidenced the absence of a volume anomaly at the phase transition, upon cooling in the absence of an applied external magnetic field, indicating that the phase transition is second order (a volume contraction is present when a first-order transition to the metallic phase is induced by cooling in a strong magnetic field). Both the PI and the CAF phases are characterized by a deviation of the thermal-expansion coefficient from the Grüneissen law, with onset in excess of 400 K. These observations lead to the hypothesis that the *local* structure is unchanged at the PI-CAF phase transition, which would then be characterized only by the long-range ordering, in the CAF phase, of structural distortions which would be already present in the PI phase. In this scenario, the JT polaron, as proposed by Millis and other authors, would not be isolated JT-distorted $Mn^{3+}O_6$ octahedra, but rather extended clusters with the same *local* structure of the charge-ordered phase, in which several JT-distorted $Mn^{3+}O_6$ and undistorted $Mn^{4+}O_6$ octahedra would form an orbitally ordered arrangement. A possible implication of such a model would be the existence of short-range magnetic correlations between the Mn ions in the cluster, which would be the precursors of the long-range magnetic ordering in the charge-ordered phases, as well as in the undistorted region between the clusters. Based on this analogy, one would expect these correlations to be predominantly *antiferromagnetic* in the distorted regions and *ferromagnetic* in the undistorted ones. This model would provide an explanation for the strong short-range magnetic fluctuations recently observed by Lynn *et al.*[37] and by De Teresa *et al.*[38] in the paramagnetic phase of these compounds.

ACKNOWLEDGMENTS

The work at Argonne was supported by the US Department of Energy, Office of Basic Energy Sciences-Materials Sciences, Contract No. W-31-109-ENG-38 (for J.D.J.) and the National Science Foundation, Office of Science and Technology Centers, Grant No. DMR 91-20000 (D.N.A.).

*Present address, LANSCE, Los Alamos National Laboratory, Los Alamos, New Mexico 87545.

[1] H. Y. Hwang, S-W. Cheong, P. G. Radaelli, M. Marezio, and B. Batlogg, Phys. Rev. Lett. **75**, 914 (1995).
[2] H. Y. Hwang, T. T. Palstra, S-W. Cheong, and B. Batlogg, Phys. Rev. B **52**, 15 046 (1995).
[3] M. C. Martin, G. Shirane, Y. Endoh, K. Hirota, Y. Moritomo, and Y. Tokura, Phys. Rev. B **53**, 14 285 (1996).
[4] P. G. Radaelli, D. E. Cox, M. Marezio, S-W. Cheong, P. E. Schiffer, and A. P. Ramirez, Phys. Rev. Lett. **75**, 4488 (1995).
[5] P. G. Radaelli, M. Marezio, H. Y. Hwang, S-W. Cheong, and B. Batlogg, Phys. Rev. B **54**, 8992 (1996).
[6] P. G. Radaelli, M. Marezio, H. Y. Hwang, and S-W. Cheong, J. Solid State Chem. **122**, 444 (1996).
[7] R. Mahesh, R. Mahendiran, A. K. Raychaudhuri, and C. N. R. Rao, J. Solid State Chem. **120**, 204 (1995).
[8] J. Foncuberta, B. Martínez, A. Seffar, S. Piñol, J. L. García-Muñoz, and X. Obradors, Phys. Rev. Lett. **76**, 1122 (1996).
[9] P. G. Radaelli, D. E. Cox, M. Marezio, and S-W. Cheong, Phys. Rev. B **55**, 3015 (1997).
[10] J. B. A. A. Elemans, B. Van Laar, K. R. Van Der Veen, and B. O. Loopstra, J. Solid State Chem. **3**, 238 (1971).
[11] P. Norby, I. G. K. Andersen, E. K. Andersen, and N. H. Andersen, J. Solid State Chem. **119**, 191 (1995).
[12] Here, as in the remainder of the paper, the standard setting *Pnma* is used to describe the orthorhombic space group adopted by $LaMnO_3$ and other compounds in the $A_{1-x}A'_xMnO_3$ system.
[13] C. Zener, Phys. Rev. **82**, 403 (1951).
[14] P. W. Anderson and H. Hasegawa, Phys. Rev. **100**, 675 (1955).
[15] P.-G. de Gennes, Phys. Rev. **118**, 141 (1960).
[16] N. Furukawa, J. Phys. Soc. Jpn. **64**, 2734 (1995).
[17] A. J. Millis, P. B. Littlewood, and B. I. Shraiman, Phys. Rev. Lett. **74**, 5144 (1995).
[18] A. J. Millis, B. I. Shraiman, and R. Mueller, Phys. Rev. Lett. **77**, 175 (1996).
[19] H. Röder, J. Zang, and A. R. Bishop, Phys. Rev. Lett. **76**, 1356 (1996).
[20] S. J. L. Billinge, R. G. Difrancesco, G. H. Kwei, J. J. Neumeier, and J. D. Thompson, Phys. Rev. Lett. **77**, 715 (1996).
[21] P. Dai, J. Zhang, H. A. Mook, S.-H. Liou, P. A. Dowben, and E. W. Plummer, Phys. Rev. B **54**, 3694 (1996).
[22] D. N. Argyriou, J. F. Mitchell, C. D. Potter, D. G. Hinks, and J. D. Jorgensen, Phys. Rev. Lett. **76**, 3826 (1995).
[23] E. O. Wollan and W. C. Koehler, Phys. Rev. **100**, 545 (1955).
[24] Z. Jirák, S. Krupicka, Z. Simsa, M. Dlouhá, and S. Vratislav, J. Magn. Magn. Mater. **53**, 153 (1985).
[25] B. Raveau, A. Maignan, and V. Caignaert, J. Solid State Chem. **117**, 424 (1995).
[26] H. Yoshizawa, H. Kawano, Y. Tomioka, and Y. Tokura, Phys. Rev. B **52**, R13 145 (1995).
[27] V. Caignaert, E. Suard, A. Maignan, C. Simon, and B. Raveau, J. Magn. Magn. Mater. **153**, L260 (1996).
[28] Y. Moritomo, A. Asamitsu, and Y. Tokura, Phys. Rev. B **51**, 16 491 (1995).
[29] J. J. Neumeier, M. F. Hundley, J. D. Thompson, and R. H. Heffner, Phys. Rev. B **52**, R7006 (1995).
[30] A. C. Larson and R. B. von Dreele, GENERAL STRUCTURE ANALYSIS SYSTEM (1985).
[31] R. D. Shannon, Acta Crystallogr. Sect. A **32**, 751 (1976).
[32] F. Moussa, M. Hennion, J. Rodriguez-Carvajal, and H. Moudden, Phys. Rev. B **54**, 15 149 (1996).
[33] C. H. Booth, F. Bridges, G. J. Snyder, and T. H. Geballe, Phys. Rev. B **54**, 15 606 (1996).
[34] L. M. Rodriguez-Martinez and J. P. Attfield, Phys. Rev. B **54**, 15 622 (1996).
[35] M. Medarde, J. Mesot, P. Lacorre, S. Rosenkranz, P. Fischer, and K. Gobrecht, Phys. Rev. B **52**, 9248 (1995).
[36] J. M. De Teresa, M. R. Ibarra, C. Marquina, P. A. Algarabel, and S. Oseroff, Phys. Rev. B **54**, R12 689 (1996).
[37] J. W. Lynn, R. W. Erwin, J. A. Borchers, Q. Huang, A. Santoro, J. L. Peng, and Z. Y. Li, Phys. Rev. Lett. **76**, 4046 (1996).
[38] J. M. De Teresa, M. R. Ibarra, P. A. Algarabel, C. Ritter, C. Marquina, J. Blasco, J. García, A. del Moral, and Z. Arnold, Nature (London) **386**, 256 (1997).